

Article

Optimization-Based Operation of District Heating Networks: A Case Study for Two Real Sites

Markus Schindler ^{1,*}, Lukas Gnam ^{2,t}, Markus Puchegger ^{1,t}, Karina Medwenitsch ^{1,t} and Patricia Jasek ^{1,t}¹ Forschung Burgenland GmbH, Campus 1, 7000 Eisenstadt, Burgenland, Austria² Fachhochschule Burgenland GmbH, Steinamangerstraße 21, 7423 Pinkafeld, Burgenland, Austria

* Correspondence: markus.schindler@forschung-burgenland.at

† These authors contributed equally to this work.

Abstract: To achieve the ambitious targets of net-zero greenhouse gas emissions by 2050, there is a need for change in all parts of society, industry, and mobility, as well as in all energy sectors. For this purpose, sector coupling plays a crucial role, e.g., in the form of coupling the electricity with the heat sector using power-to-heat systems. In this article, the effects of the integration of intermittent wind energy via a direct cable, as well as the integration of a boiler into district heating systems powered by a biomass plant and/or a gas boiler, are investigated. Sector coupling in the district heating networks is achieved via the integration of a boiler connected to a local grid station and the use of two air-to-water and two water-to-water heat pumps, which are solely powered by electricity produced by local wind turbines. Furthermore, this work evaluates the economic impacts of the exploding energy prices on the sustainability of district heating systems. Our analysis shows that despite high electricity prices, a reduction in fossil-fuel-based energy generators in the winter season can be determined, and thus a sustainable heat supply can be ensured.

Keywords: district heating; renewable energy sources; mixed-integer linear problem; optimization; unit commitment



Citation: Schindler, M.; Gnam, L.; Puchegger, M.; Medwenitsch, K.; Jasek, P. Optimization-Based Operation of District Heating Networks: A Case Study for Two Real Sites. *Energies* **2023**, *16*, 2120. <https://doi.org/10.3390/en16052120>

Academic Editors: Francesco Calise, Neven Duić, Poul Alberg Østergaard, Qiuwang Wang and Maria da Graça Carvalho

Received: 14 January 2023

Revised: 10 February 2023

Accepted: 16 February 2023

Published: 22 February 2023



Copyright: © 2023 by the authors. Licensee MDPI, Basel, Switzerland. This article is an open access article distributed under the terms and conditions of the Creative Commons Attribution (CC BY) license (<https://creativecommons.org/licenses/by/4.0/>).

1. Introduction

The decarbonization of the energy system is absolutely crucial for the global economy to become climate-neutral. The European Green Deal has proclaimed the goals to achieve net-zero CO₂ emissions by 2050 and to decouple economic growth from resource use for Europe [1]. An essential cornerstone for achieving these goals was accomplished in Austria with the Renewable Expansion Act, which sets the essential framework conditions for the decarbonization of the energy sector [2]. Among other aspects, this law sets the goal of completely decarbonizing the generation of electricity in Austria by 2030. Other energy sectors are to follow by 2040, with the use of sector-coupling options via volatile renewable electricity sources playing a key role in achieving this goal. Burgenland, the easternmost state of Austria, already has a balance surplus of renewable electricity due to its generation structure based on wind energy [3]. By 2030, photovoltaic (PV) capacity is to be ramped up in the same order of magnitude as wind energy. This means that in this state, there already are, or will be in the near future, framework conditions that enable the use of sector-coupling approaches and thus the decarbonization of all energy sectors. Figure 1 shows both the electricity production (grey line) and consumption (orange area) in Burgenland over a period of 30 days in January 2023.

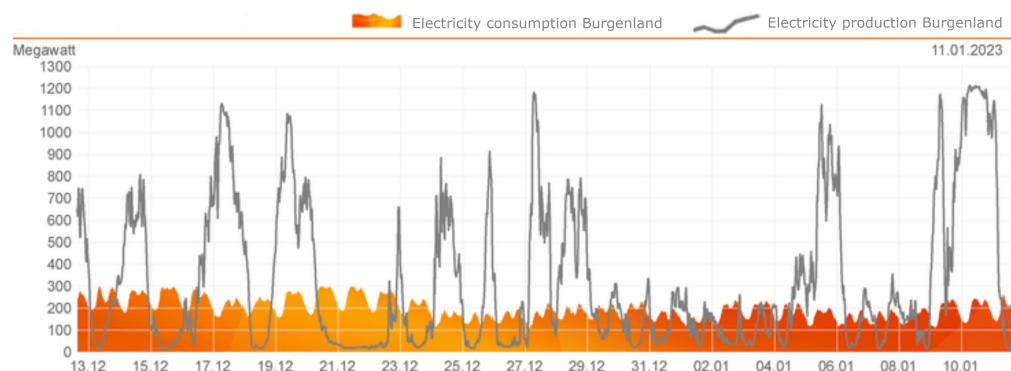


Figure 1. Electricity consumption and production in Burgenland over 30 days in December 2022/January 2023 (modified: translated from German to English) [3].

This figure shows that during the production peaks of up to more than 1 GW, a large surplus of renewable production of approximately 800 MW is achieved, whereas during wind lulls, production is not able to cover consumption at all.

The economic value of surplus wind energy can be increased by integrating it into the heating sector [4]. In the district heating sector, in particular, the development of large heat pumps (HPs) has offered an interesting opportunity for the use of wind energy in these systems [5]. In addition, converting electricity into thermal energy enables the use of highly efficient and cost-effective thermal energy storage systems [6]. If such plants could be operated with district heating based on renewable energy sources, it would be necessary to check their economic feasibility in the long run. Ideally, such systems would achieve lower heat production costs than conventional heat generators such as gas boilers (GBs). The operation of such power-to-heat (PtH) plants heavily depends on two main factors: the regulatory framework on the one hand and the current electricity exchange prices on the other hand. The latter determine the opportunity costs for the operation of the plants. Furthermore, if the energy transport from the wind park to the PtH plant is carried out via the public electricity grid, further grid fees apply, which jeopardize potential revenues. Hence, one option is to directly connect the wind park to the PtH plant.

Considering the overall conditions described above, this paper shows numerical examples of established methods for the realization of power-to-heat integrating district heating networks (DHNs). Furthermore, the operational behaviors of two existing PtH plants located in the Burgenland towns of Oberwart and Neusiedl am See are investigated by using mixed-integer linear programming (MILP) to model the two DHNs under investigation. The latter DHN has the special property that the PtH plant, i.e., its HPs, are directly connected to a local wind park and solely powered with wind energy. In addition, a comparison is made between the operational behavior of the second DHN in Neusiedl am See in the period 2019–2020 and 2022, given that the electricity prices in 2022 considerably differed from those in 2019–2020.

This paper is organized as follows: In Section 2, the current state of research regarding DHNs and PtH plants is described. In Section 3, the structure of the studied DHNs and their performance parameters are depicted. In Section 4, the methodology including the modeling of the energy systems is presented. In addition, one of the energy systems is remodeled with updated data, taking the increased gas and electricity prices of the year 2022 into consideration. The mathematical descriptions of the individual components of the modeled energy systems follow in the subsections of this chapter. In Section 5, the results of the optimization models are presented and discussed. In Section 6, the key statements of this article are summarized and a final conclusion is made.

The novelty of this article lies in the realization of coupling the heat and electricity sector, utilizing a boiler and HPs, with the latter not being connected to the public electricity grid. Therefore, the second DHN's unit commitment has to be optimized in order to

optimally integrate wind energy. Subsequently, the use of fossil-fueled heat generators as well as the operational costs of the DHN are minimized. Another new approach is the comparison of these investigations to the economic circumstances of the year 2022, given that the electricity exchange prices have increased significantly since 2019, and the economic feasibility of such PtH plants has to be analyzed anew.

2. Current State of Research

Since sector coupling plays an essential role in the course of transforming our energy systems, much research effort was dedicated to different approaches in connection with PtH plants. Lamaison et al. studied the influence of storage systems on a DHN with combined production from a biomass boiler and a PtH plant [7]. They proved that the present district heating demand in various DHNs in France can sufficiently be provided by biomass plants (BMPs) in combination with HPs and storage solutions. An example of the application of MILP in power-system modeling is the work of Wirtz et al. [8], where a MILP model was developed for a fifth-generation DHN, based on bidirectional low-temperature networks. The authors showed that following this low-temperature approach, a cost reduction of 42% would be achieved. Furthermore, the developed model can be used for predictive control due to its real-time capability. In Quaggiotto et al. [9], the authors modeled a DHN powered with HPs, combined heat and power plants, and GBs. Their MILP optimization based on a two-week rolling horizon revealed that operational costs for one week of operation could be reduced by up to 20% when installing additional thermal storage. The impacts of wind power on thermal generation unit commitment and dispatch were studied by Ummels et al. [10]. In this publication, the authors stated that the integration of wind energy only into a thermal system is not trivial due to the intermittent generation characteristics of wind energy and the minimum load issues. Furthermore, Zheng et al. investigated an equivalent model-based non-iterative solution for efficient coordination between different energy sectors while maintaining privacy in the distributed operation of integrated electricity and heat systems [11]. However, their model requires cooperation between the energy sectors. Zheng and Hill dealt with the distributed real-time dispatch of integrated electricity and heat systems with guaranteed feasibility [12]. A MILP formulation can also be used for the optimal control of combined heat and power plants, which is shown in [13]. The presented approach was verified using test data from two turbines for coupled and decoupled approaches combining heat and power generation components. In Ref. [14], a design procedure for a fifth-generation DHN based on a linear programming approach was presented. The approach was tested on two real German sites with individual heating, ventilation and air conditioning systems. The results showed a cost reduction of 42% and a reduction in CO₂ emissions by 56%. In Ref. [15], a tool for the topology analysis of fifth-generation district heating systems was developed. This paper focused on the development of a hydraulic model to calculate the optimal network for a given district. Barone et al. developed a dynamic simulation model for the modeling and optimization of the thermo-economic analysis of a district heating system [16]. With their model, the authors revealed that energy savings of up to 17% are possible. Li et al. [17] proposed a model of an integrated electricity and district heating system based on the thermal inertia of the heating network and the buildings on the demand side. However, their model results in a quadratic programming problem.

3. Modeled Heat Production Scenarios

As mentioned before, both investigated DHNs are located in the Austrian state of Burgenland. The climate in Burgenland is classified as a humid continental climate with four distinct seasons. In winter, temperatures can drop to below freezing, with snow and frost being common. The average temperature in January, the coldest month, is around 1.3 °C [18]. During summer, the average temperature is at around 22.4 °C [18] in July. Precipitation is fairly consistent throughout the year, with an average of 551 mm per year [18]. The region is known for its frequent thunderstorms, particularly during the

summer months. Wind patterns in Burgenland are predominantly westerly, with occasional east and northeast winds. In summer, the winds tend to be light and variable, while in winter, they can be stronger and gustier. Burgenland's topography has a significant impact on the local climate, with the low-lying areas near lake Neusiedler See being particularly susceptible to fog and cloud formation. Higher elevations, such as the hills surrounding the lake, tend to have clearer weather conditions.

The first district heating network (DHN1) considered in this article, displayed in Figure 2, is located in the Burgenland town of Oberwart and consists of a BMP, which feeds the DHN via a heat storage unit. As part of a former research project, the plant was extended by a PtH unit in form of a boiler, which consumes electricity from the local grid station. This connection to the public grid results in additional grid fees for the operation of the boiler. All the presented parameters that do not contain additional references were provided by the operating company [3] for both investigated sites.

For the cost efficiency calculations of DHN1, the following parameters were used: In general, the necessary data sets for temperature, heat demand, and electricity prices from the period between 1 September 2019 and 31 August 2020 were applied. An efficiency of $\eta = 0.91$ was assumed for the BMP. In the optimization, the initial thermal power of the BMP was at $P_{init} = 500$ kW. The initial values for the other parameters of the DHN were set according to the heat demand of the initial time step. The lower operating limit was assumed to be $P_{min} = 500$ kW, whereas the maximum power was assumed to be $P_{max} = 5.8$ MW. In addition, the power production could be increased to a maximum of $P_{gradmax} = 4.5$ MW/h. The energy price for the BMP was defined as $p = 2$ ct/kWh. The PtH plant was set with a maximum thermal power of $Q_{max} = 350$ kW. As for the time series denoting the electricity price, the time period from 1 September 2019 to 31 August 2020 was chosen. The individual day-ahead electricity prices were taken from the electricity exchange EXAA [19]. In addition, consumption-dependent grid usage fees amounting to 3.327 ct/kWh were taken into consideration. This fee is composed of a grid usage fee for interruptible loads in the amount of 1.4 ct/kWh, a grid loss fee in the amount of 0.07 ct/kWh, a green electricity subsidy in the amount of 0.352 ct/kWh and an electricity duty amounting to 1.5 ct/kWh. The described DHN in Oberwart had a maximum heat demand of 4761.59 kW with an average heat load of 1547.65 kW and a standard deviation of 891.02 kW.

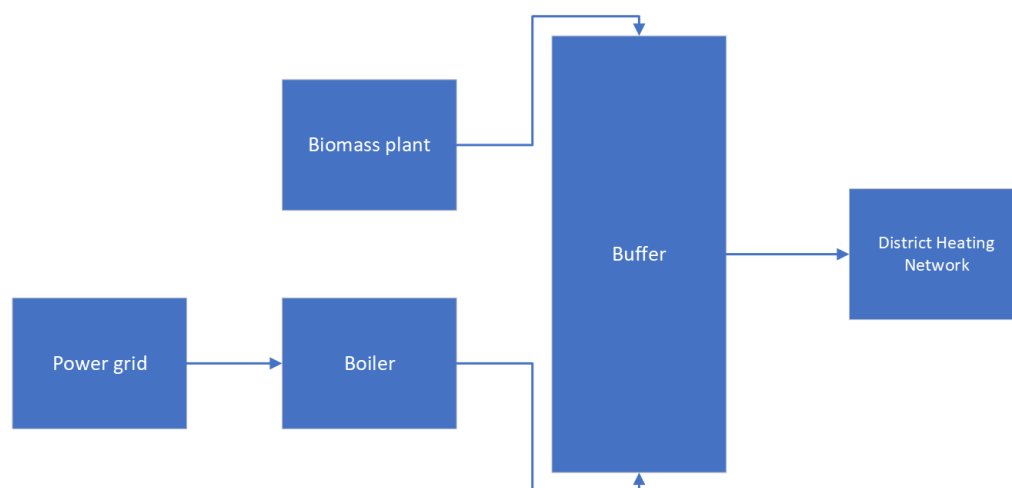


Figure 2. Structure of DHN1 located in Oberwart, Austria.

The second DHN (DHN2) considered in this paper is located in Neusiedl am See in the Austrian province of Burgenland and is displayed in Figure 3. It originally consisted of a BMP and a GB, which both fed the DHN via a buffer. Due to the vicinity of the DHN to a local wind farm with 30 MW peak power, it was decided to expand the DHN by a HP cascade consisting of two air-to-water and two water-to-water HPs, which also feed

into the buffer. The power used for the operation of the HPs is directly drawn from the wind park via a direct cable, which was installed at the time the HPs were added, as the investment costs for this construction were predicted to be lower than the accumulating grid usage costs in the long term. Additionally, a flue gas condenser was added to the BMP. The system has different operating modes for summer and winter: In summer mode, the BMP is switched off. During this period, the air-to-water HPs use ambient air to feed into the so-called cold storage tank. The temperature increase from the cold storage tank to the hot storage tank is achieved using the water-to-water HPs. In winter mode, the BMP is in operation, and the air-to-water HPs feed directly into the hot storage tank, whereas the cold storage tank is supplied by the flue gas condenser of the BMP. By means of this upgrade of the DHN, the GB is only planned to serve as a backup system in case of wind lulls or to compensate for the inertia of the BMP. The switch from one mode to the other is predetermined by the plant operator and thus was not implemented as a variable in our MILP model.

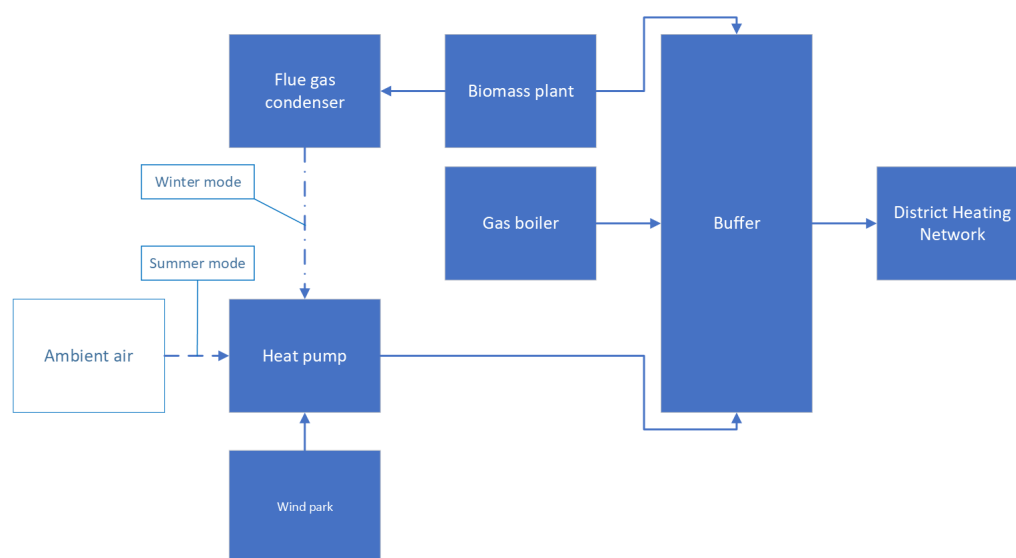


Figure 3. Structure of DHN2 located in Neusiedl am See, Austria.

Regarding cost-minimizing calculations, the data sets concerning wind production, temperature, heat demand, and electricity prices from the entire year of 2019 were used. The parameters for DHN2 were set as follows: The BMP was modeled with power limits of $P_{min} = 520$ kW and $P_{max} = 2600$ kW. The maximum change in power production per hour was thereby $P_{gradmax} = 780$ kW. The biomass price in this system was assumed to be $p_f = 4$ ct/kWh. The time period from 1 January 2019 to 31 December 2019 was chosen for the time series denoting the electricity price. Equivalent to DHN1, the day-ahead prices used in this study were taken from the electricity exchange EXAA [19]. As mentioned before, the GB is mainly used as a reserve. The GB could output a maximum power of $P_{max} = 3.9$ MW, and the efficiency of the system was defined as $\eta = 0.93$. The gas price in this model was assumed to be at $p_g = 15$ ct/kWh. This parameter was deliberately set higher than it was in reality in order to ensure that the GB only served as a backup system as planned. The maximum capacity of the buffer was assumed to be 300 m^3 . The HPs were modeled with a maximum thermal power of $Q_{max} = 2$ MW. The maximum heat demand of the described DHN was 5290 kW with an average heat load of 1706.43 kW, where the standard deviation was 1091.61 kW.

When these calculations were first conducted in late 2021, the economic situation was rather stable. However, since then, several developments, such as the economic consequences of the COVID-19 pandemic and the Russian–Ukrainian war, have undeniably had a huge impact on price increases, especially when it comes to gas and electricity prices. Figure 4 shows a comparison between the day-ahead price in 2019 and 2022 in ct/kWh.

While the prices in 2019 remained relatively stable at around 12–15 ct/kWh, some day-ahead prices in 2022 increased to even beyond 100 ct/kWh, while most of the year they were between 18 and 35 ct/kWh. This means that in comparison to 2019, the electricity price was twice to three times as high during a great part of 2022. Naturally, this also impacts the heat production costs in DHNs. Therefore, another scenario including the change in these parameters is included in this paper. The calculations performed for DHN2 were carried out again by using the updated data from 2022. In detail, the gas price was adapted to the increase in the Austrian gas price index (which increased by a factor of 7.5 from 2019 to 2022 based on a yearly average) [20] (Figure 5) and the biomass price (which increased by a factor of 1.3 from 2019 to 2022) was adapted to the biomass index [21]. For 2022, the maximum heat demand was 5725 kW, with an average heat demand of 1423.39 kW and a standard deviation of 806.4 kW.

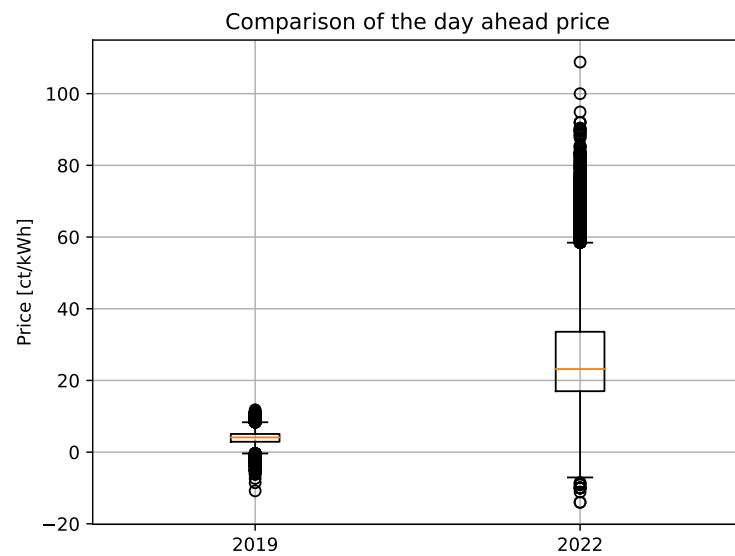


Figure 4. Comparison of the electricity prices in 2019 and 2022.

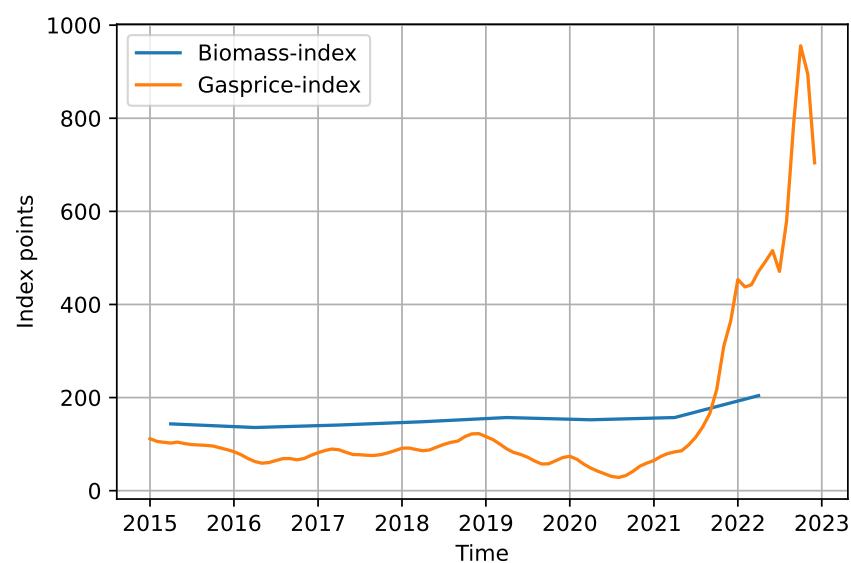


Figure 5. Austrian gas price index (monthly base) [20] and upper Austrian biomass index [21].

4. Investigation Method

In this section, the mathematical modeling of energy systems is explained. The models presented in this paper are formulated using the MILP framework. This MILP method was chosen because it is a standard method in the field of unit commitment. The advantages of this method are the widely available commercial or open-source solvers and modeling tools. This allows researchers to focus on model development. To keep the modeling of energy systems consistent, an object-oriented modeling approach was chosen. Here, the behavior of each component, such as the HP or the BMP, is represented by a separate block. Based on the resulting building blocks, the energy systems can be generated with the help of further constraints. This object-oriented modeling approach was implemented via the utilization of the Pyomo framework [22]. There already exist many frameworks for mathematical optimization which focus on the energy sector in the scientific community. An example is the Oemof [23] framework. However, we believe that these frameworks either represent very basic functionality, such as the Pyomo framework, or abstract the problem very far, such as Oemof. Our internal MILP framework “ESMAS” (Energy System Modeling And Simulation) is exactly in between and offers the possibility to abstract elements such as HPs or BMPs. At the same time, it is still possible to add model extensions on equation level. The functionalities as well as the structure of the ESMAS framework are displayed in Figure 6.

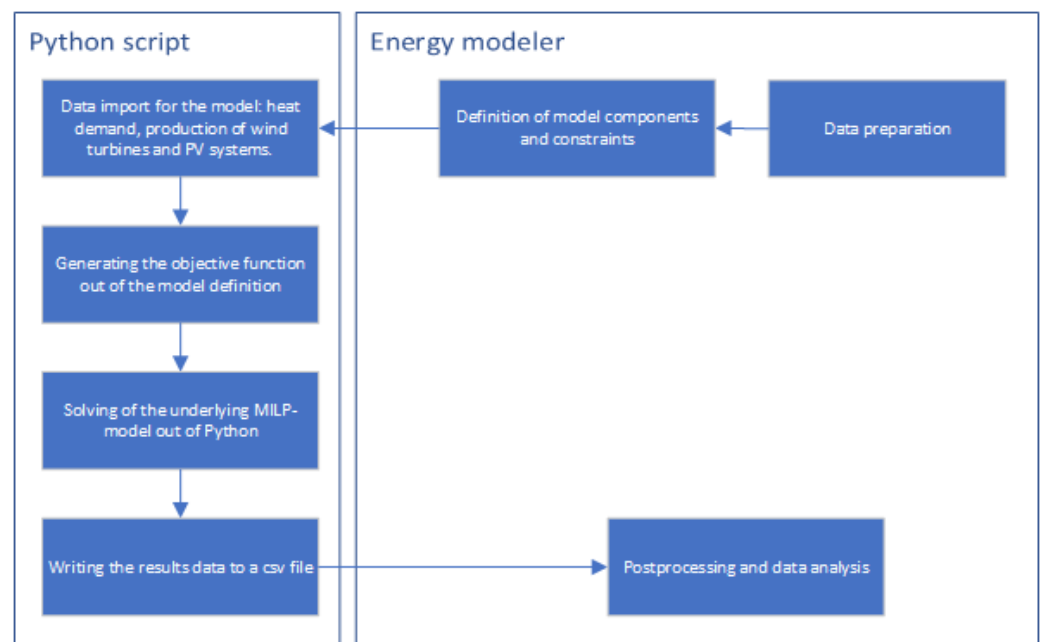


Figure 6. Functionality and structure of the ESMAS (energy system modeling and simulation) framework.

The two DHNs are composed of the individual components the ESMAS framework offers. The following components, among others, are provided by ESMAS to model the DHNs: a BMP, a boiler, a GB, a HP, a storage, and a grid component. The relations between the individual components are built into the model via additional constraints. Essentially, these are equation constraints that ensure that the conservation of energy between the various components is valid. This ensures that the individual components are available as building blocks. The energy system modeler creates as many instances of these building blocks as necessary. The advantage of this method is that it guarantees the same behavior for all submodels. The objective function for the optimization model is an operational expenditure (OPEX) function. This function is automatically built out of the OPEX functions from every subcomponent. For all the calculations performed in this article, time is assumed to be discrete. The period I studied is divided into constant intervals t .

In the following subsections the components provided by the ESMAS framework and used in the optimization model are described in detail.

4.1. Heat Pump

The coefficient of performance COP^{hp} of the HP is either fixed or a series of values that is calculated before the optimization run based on time-series data for the temperature. For the HP, the relationship between the absorbed electrical power P_{el}^{hp} at the time i and the delivered thermal power P_{th}^{hp} at the time i is described by (1), depending on the type of COP^{hp} .

$$P_{th}^{hp}(i) = COP^{hp}(i) \cdot P_{el}^{hp}(i) \quad \forall i \in I \quad (1)$$

The maximum electric power of the HP is defined by Equation (2), where $P_{el,max}^{hp}$ is the limiting factor for the maximum power, and σ^{hp} is the binary variable defining whether the HP is turned on or off at the time i .

$$P_{el}^{hp}(i) \leq P_{el,max}^{hp} \cdot \sigma^{hp}(i) \quad \forall i \in I \quad (2)$$

4.2. Storage

The state of charge SOC^{sto} of the heat storage at the time i is calculated using the recursion Equation (3) from the state of charge SOC^{sto} from the previous time step $i - 1$ and the difference in inflows SOC_{charge}^{sto} and outflows $SOC_{discharge}^{sto}$ from the previous time step $i - 1$.

$$SOC^{sto}(i) = SOC^{sto}(i - 1) + t \cdot (SOC_{charge}^{sto}(i - 1) - SOC_{discharge}^{sto}(i - 1)) \quad \forall i \in I \quad (3)$$

In Equation (3), storage losses are not considered because storage capacities are not sufficient to store more energy for more than one day. The boundaries for the SOC^{sto} as well as for its inflows SOC_{charge}^{sto} and outflows $SOC_{discharge}^{sto}$ are implemented using Equations (4)–(6).

$$SOC_{min}^{sto} \leq SOC^{sto}(i) \leq SOC_{max}^{sto} \quad \forall i \in I \quad (4)$$

$$SOC_{charge,min}^{sto} \leq SOC_{charge}^{sto}(i) \leq SOC_{charge,max}^{sto} \quad \forall i \in I \quad (5)$$

$$SOC_{discharge,min}^{sto} \leq SOC_{discharge}^{sto}(i) \leq SOC_{discharge,max}^{sto} \quad \forall i \in I \quad (6)$$

The $SOC_{charge,max}^{sto}$ is calculated using the specific heat capacity, the volume, and the temperature difference ΔT , which is caused by the DHN. ΔT is also the control variable for the closed-loop control and can be assumed to be constant for our considerations.

4.3. Biomass Plant

The objective function of the BMP is defined as the $OPEX^{bmp}$ Function (7), where P_{th}^{bmp} is the produced thermal power of the BMP, C^{bmp} is the biomass price in ct/kWh⁻¹, C_{up}^{bmp} are the costs for starting up the BMP, C_{down}^{bmp} are the costs for shutting down the BMP, δ^{bmp} is the binary variable for whether the BMP is in operation or not (δ_{up}^{bmp} or δ_{down}^{bmp}), η^{bmp} is the overall efficiency of the BMP, i marks a specific time, and t is the time step of the optimization.

$$OPEX^{bmp} = t \cdot \frac{\sum_i^I P_{th}^{bmp}(i) \cdot C^{bmp}(i)}{\eta^{bmp}} + C_{up}^{bmp} \cdot \sum_i^I \delta_{up}^{bmp}(i) + C_{down}^{bmp} \cdot \sum_i^I \delta_{down}^{bmp}(i) \quad (7)$$

For ember conservation, the BMP has a minimum power $P_{th,min}^{bmp}$ to produce when it is on. This is modeled using (8).

$$P_{th,min}^{bmp} \cdot \sigma^{bmp}(i) \leq P_{th}^{bmp}(i) \quad \forall i \in I \quad (8)$$

The thermal power produced while the BMP is in operation is restricted by the maximum thermal power $P_{th,max}^{bmp}$, as displayed in (9).

$$P_{th}^{bmp}(i) \leq P_{th,max}^{bmp} \cdot \sigma^{bmp}(i) \quad \forall i \in I \quad (9)$$

The gradient of the provided thermal energy is modeled using Equations (10) and (11). Here, $P_{grad,max}^{bmp}$ is the maximum gradient between two time steps.

$$P_{th}^{bmp}(i) - P_{th}^{bmp}(i-1) \leq t \cdot P_{grad,max}^{bmp} \quad \forall i \in I \quad (10)$$

$$P_{th}^{bmp}(i-1) - P_{th}^{bmp}(i) \leq t \cdot P_{grad,max}^{bmp} \quad \forall i \in I \quad (11)$$

For the first time step, the limitation of change in the thermal power is modeled using Equations (12) and (13), where $P_{th,init}^{bmp}$ is the initial value of the BMP, which is set to the value $P_{th,min}^{bmp}$.

$$P_{th}^{bmp}(i) - P_{th,init}^{bmp} \leq t \cdot P_{grad,max}^{bmp} \quad \forall i \in I \quad (12)$$

$$P_{th,init}^{bmp} - P_{th}^{bmp}(i) \leq t \cdot P_{grad,max}^{bmp} \quad \forall i \in I \quad (13)$$

4.4. Boiler

The relationship between the thermal power output P_{th}^{boiler} and the electrical power consumed P_{el}^{boiler} is described by the efficiency η and is represented by Equation (14).

$$P_{th}^{boiler}(i) = P_{el}^{boiler}(i) \cdot \eta \quad \forall i \in I \quad (14)$$

The maximum value of P_{th}^{boiler} is limited by (15) using the parameter $P_{th,max}^{boiler}$.

$$0 \leq P_{th}^{boiler}(i) \leq P_{th,max}^{boiler} \quad \forall i \in I \quad (15)$$

4.5. Gas Boiler

The GB is modeled using the OPEX^{gb} Equation (16), where P_{th}^{gb} is the produced thermal power of the GB, C^{gb} is the gas price in ct/kWh, and η^{gb} is the degree of efficiency of the system. There is also an additional equation to limit the thermal power to the value $P_{th,max}^{gb}$.

$$\text{OPEX}^{gb} = t \cdot \frac{\sum_i P_{th}^{gb}(i) \cdot C^g(i)}{\eta^{gb}} \quad \forall i \in I \quad (16)$$

4.6. Power Grid

The power grid is used to model the pricing constraints of the Austrian day-ahead energy market. In Equation (17), $P_{el,in}^{grid}$ is the procured energy from the grid, $P_{el,out}^{grid}$ is the energy that is fed into the grid, and C_{el} is the electricity price.

$$\text{OPEX}^{grid} = t \cdot \sum_i P_{el,out}^{grid}(i) \cdot C_{el}(i) - t \cdot \sum_i P_{el,in}^{grid}(i) \cdot C_{el}(i) \quad (17)$$

To eliminate the possibilities that $P_{el,out}^{grid}(i) > 0$ and $P_{el,in}^{grid}(i) > 0$ at the time step i , additional constraints (18)–(20) are added for every time step i .

$$\sigma_{in}(i) + \sigma_{out}(i) \leq 1 \quad \forall i \in I \quad (18)$$

$$P_{el,in}^{grid}(i) \leq P_{el,max} \cdot \sigma_{in}(i) \quad \forall i \in I \quad (19)$$

$$P_{el,out}^{grid}(i) \leq P_{el,max} \cdot \sigma_{out}(i) \quad \forall i \in I \quad (20)$$

5. Results

For the first investigated district heating network DHN1, Figure 7 shows the produced thermal power of the BMP over the course of the selected time. It can be seen that most of the required heat is produced by the BMP. In addition, the seasonal characteristic is depicted nicely in this graph. It is obvious that far more energy is produced in winter than in summer. This is due to the fact that, naturally, more heat production is needed in winter than in summer. The heat needed in summer is mainly used for hot water production, whereas in winter, the demand for heating has to be taken into consideration. A closer look at the operation of the PtH system shows that it can only be operated economically to a limited extent. In the period of investigation, the system comes to an operating time of 17 h. The simulation shows that this is only the case when the day-ahead electricity price falls below the limit of $-1.15 \text{ ct/kWh}^{-1}$. This fact is displayed in Figure 8, where the correlation between the produced power of the PtH plant and the day-ahead price (excluding grid usage fees) is depicted. Given the current market situation, where there is an increasingly less extent of negative electricity prices, the use of this system is therefore not very economic.

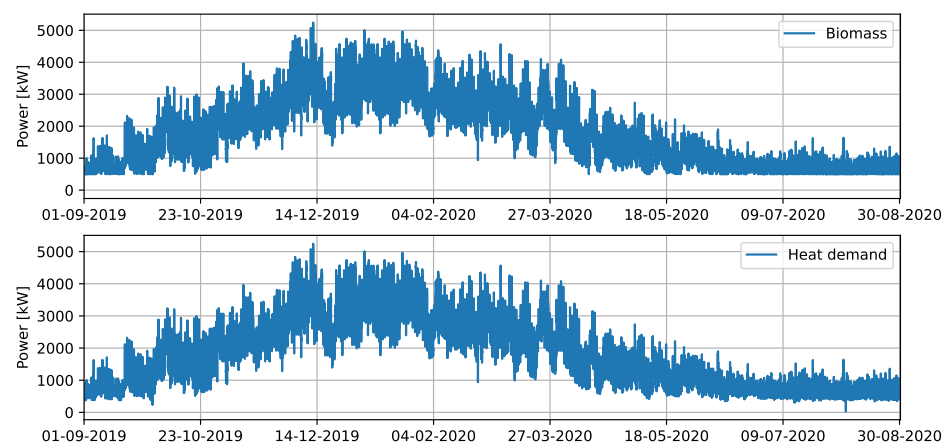


Figure 7. Operation of the BMP in Oberwart.

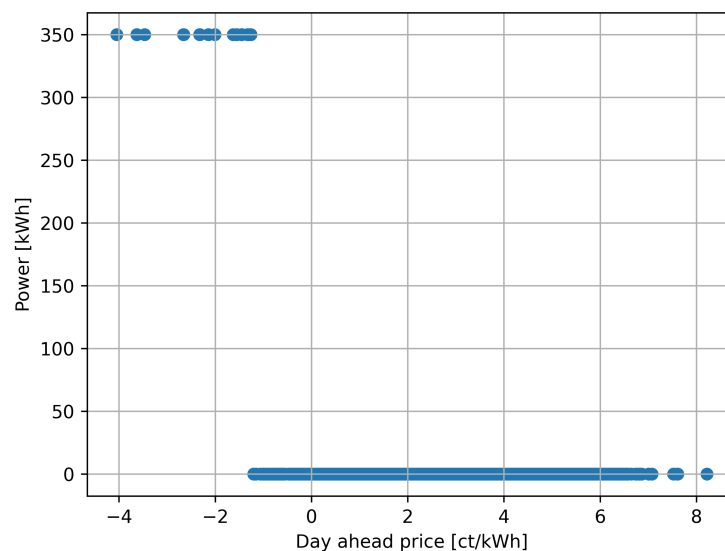


Figure 8. Operation of the PtH system in Oberwart.

In the second district heating network considered, DHN2, the situation is quite different since apart from the BMP, there are two other heat sources available. For each of the two calculated scenarios (2019 and 2022), the average daily production was determined in order to show the production characteristics. These data are displayed in Figure 9, where the produced thermal power per heat source is shown based on quarter-hourly values. It can be seen that regarding gas production, no relevant peaks can be detected on a daily basis, which is due to the fact that the GB only serves as a backup system. In the production curve of the HPs and the BMP, a characteristic with two daily peaks is detectable: The first peak tends to occur in the early morning and the second one in the afternoon. It is also remarkable that the two curves lie very well on top of each other, with production values ranging from about 400 kW to 1200 kW per quarter-hour. While the production curve from the BMP is mostly rather stable, the graph shows that the thermal power produced by the HPs is extremely volatile within short periods of time throughout the day. This is probably due to the unstable wind conditions, as the HPs in DHN2 are mainly dependent on the energy produced in the local wind park.

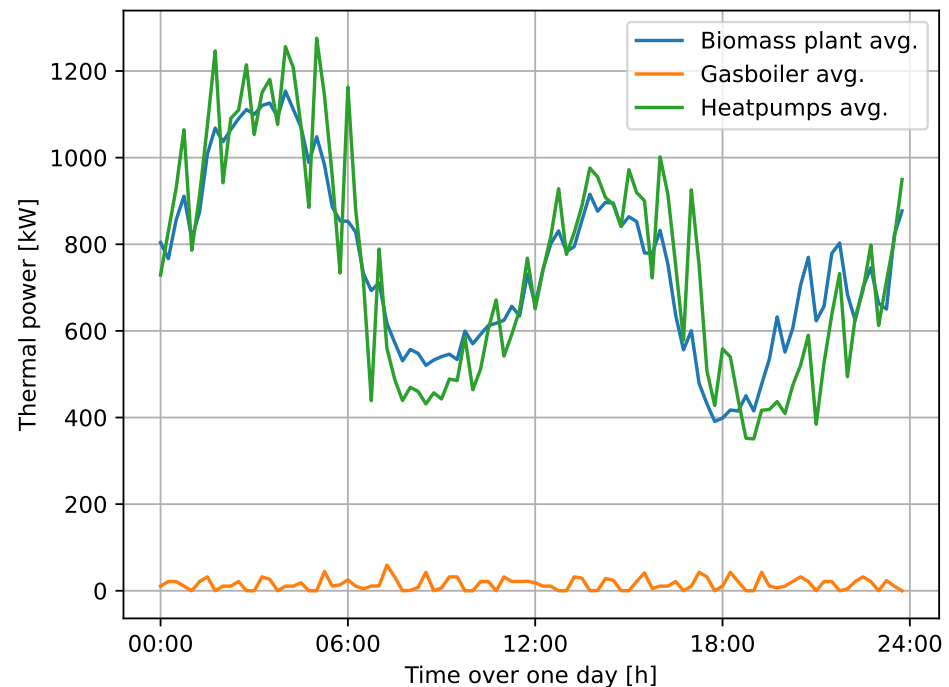


Figure 9. Average daily production of the different heat sources in Neusiedl in 2019.

For the year 2022, the results (Figure 10) look very much alike, and a similar characteristic is recognizable. As for the average daily production in 2019, the daily peaks of the BMP and HP production can be determined in the morning and in the afternoon. Furthermore, the volatility of these two curves is similar to the 2019 scenario. However, the main difference between the 2022 graph and the 2019 graph is that the production curves of the BMP and the HPs are no longer superimposed. The share of heat production by HPs was significantly lower in 2022 than in 2019, as can be seen in Figure 11. In addition, the range of the produced kW per quarter-hour was significantly lower for both the BMP and the HPs, with production ranging from about 800 kW to 1100 kW for the BMP and around 200 kW to 800 kW for the HPs. With regard to gas production, the share of heat produced by the GB in 2022 was considerably higher than in 2019. Moreover, minor production peaks can be detected in the morning and evening. In addition, the production curve of the GB is more flattened in comparison to its equivalent in 2019. In Figure 11, a comparison between the shares of the three different heat sources in 2019 and 2022 is made. While in 2019, the amount of thermal power produced by the BMP and the HPs was fairly balanced, in 2022, a larger share of heat produced by the BMP at the expense of HP production could be

detected. The decrease in the usage of the HPs was caused by the high electricity prices as well as the decreased electricity production, which dropped by 16.3% in 2022 compared with 2019. In contrast, the favorable biomass price resulted in the fact that the BMP was the best option for heat production in 2022. In addition, a higher share of gas usage is shown, which was the result of more wind lulls.

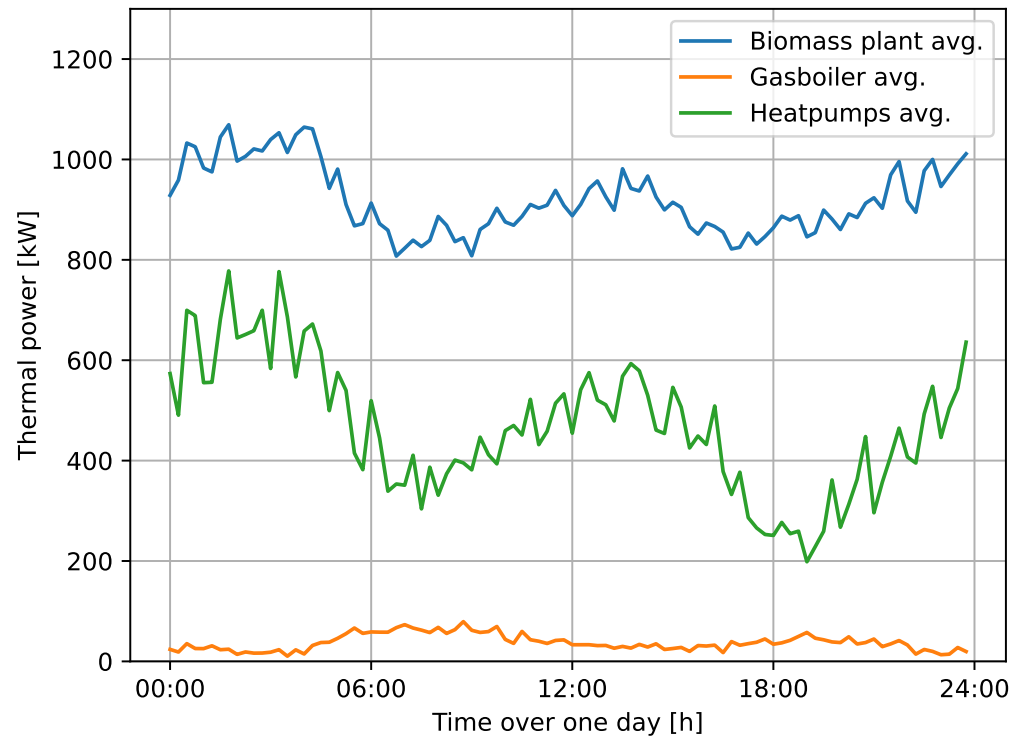


Figure 10. Average daily production of the different heat sources in Neusiedl in 2022.

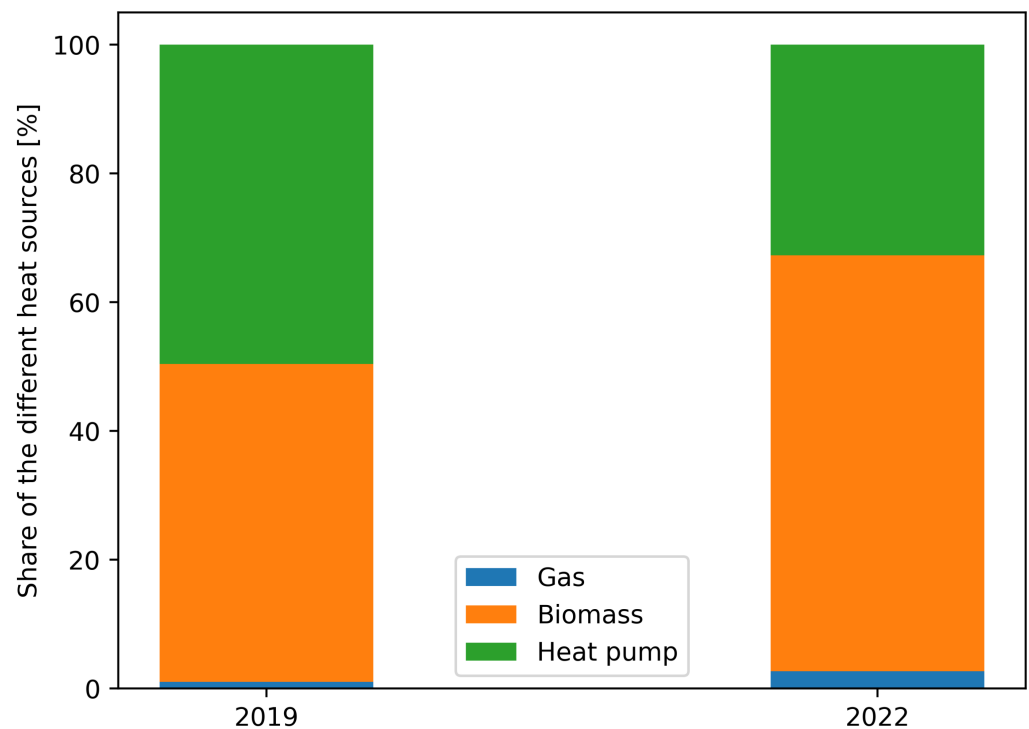


Figure 11. Comparison of the years 2019 and 2022.

As can be seen in Table 1, nearly two and a half times more gas was used for heat production in 2022 than in 2019. This is because in 2022, there was significantly less wind than in 2019, which resulted in the fact that the HPs could not be used as often as in 2019, and therefore the GB had to serve as a backup system more frequently. Interestingly, in winter, no gas was used for heat production at all, so the increased gas consumption in 2022 only occurred in summer.

Table 1. Comparison of gas usage in the different years and modes.

	2019	2022
Summer	132,752.99 kWh	330,124.64 kWh
Winter	1361.27 kWh	0.00 kWh

6. Conclusions

Both DHNs considered in this work were formulated as MILP models and then solved with the corresponding parameterization. The results obtained for both systems were quite different. In the first system studied, it was shown that the boiler produces heat only a few short times throughout the year. This only occurs when the electricity price falls below a certain threshold. This effect is intensified by the fact that grid usage fees are incurred. In order to make the first system more sustainable, the authors believe the following two main elements should be considered: Firstly, it should be investigated how the situation changes when the boiler is replaced by a HP, since this way three to four times more district heating can be produced with the same electrical installed power. The second possibility is to evaluate the installation of a PV plant in the vicinity of the heating plant. By means of this installation, the PtH plant could be supplied with the energy generated by the PV system with a direct cable, which would be more cost-efficient.

In the second plant considered, the analysis of the 2019 scenario shows that a significant proportion of the produced heat can be supplied by the HPs. In the summer mode, with the exception of a few times, the entire energy is produced by the HPs. Surely, one reason for this is the much higher efficiency of an HP compared with a conventional boiler. The HP solution also ensures that the district heating production is much more climate-friendly since considerable amounts of biomass and CO₂ can be saved.

The results for the year 2022 of the second DHN are very interesting. Despite the enormous increase in gas prices, gas consumption increased significantly. However, it is important to note that this increase in gas consumption is only seen in the summer, as in this period, the BMP is switched off and therefore not available. In addition, in contrast to 2019, in 2022 gas usage was eliminated completely in winter. This fact shows that there is still a need for optimizing the behavior of this DHN, especially in summer. Therefore, a connection of the HPs to the local grid station should be considered here. This would allow more heat to be generated by the HPs, especially in summer. However, in this case, grid usage fees could incur, which is why calculations or simulations should be made beforehand in order to determine the cost-efficiency of such a district heating system. Another possibility for enhancing HP usage in DHN2 could be the installation of a PV plant nearby. The energy produced by the PV could feed the HPs via a direct cable, allowing the district heating system to avoid grid usage fees. This measure would be particularly reasonable taking into consideration that the power provided by the PV plant would mainly be used in summer in order to replace the heat production with gas.

The studies presented here show that on the one hand, the decarbonization of DHNs is a technical problem, e.g., concerning the development of large PtH systems. On the other hand, however, the regulatory framework is a much greater hurdle. Since these regulatory constraints, as well as the political and climatic circumstances, can change from region to region, it is necessary to conduct studies such as those presented in this article. As shown in this study, modular, object-oriented modeling is particularly suitable for this purpose. The results in this paper are applicable for estimating the potential of PtH plants in DHNs.

Such PtH plants are perfectly suited for coupling the heat with the power sector. Based on the models developed here, a system for the predictive operation of DHNs can be derived in a small amount of time. This allows any surpluses from renewable electricity production to be utilized. Future research efforts will focus on the detection of the optimal switching point from summer to winter mode and vice versa since this is crucial for minimizing the use of gas. Moreover, the addition of PV plants to the DHNs that feed the HPs via a direct cable will be investigated. Furthermore, the integration of the optimization model into the operational system of the DHN operator is a major issue to further accelerate the decarbonization of the energy system in the state of Burgenland.

Author Contributions: Conceptualization, M.S. and L.G.; methodology, M.S. and L.G.; software, M.S., L.G. and K.M.; validation, M.S. and M.P.; data curation, M.P. and P.J.; writing—original draft preparation, M.S.; writing—review and editing, K.M. and L.G.; visualization, M.S.; supervision, L.G.; project administration, P.J.; funding acquisition, M.P. All authors have read and agreed to the published version of the manuscript.

Funding: This project is supported by funds from the Climate and Energy Fund and carried out within the framework of the Energy Research Program 2018.

Data Availability Statement: Restrictions apply to the availability of these data. Data was obtained from Burgenland Energie AG.

Conflicts of Interest: The authors declare no conflict of interest.

Abbreviations

The following abbreviations are used in this manuscript:

DHN	District heating network
PtH	Power to heat
MILP	Mixed-integer linear programming
HP	Heat pump
BMP	Biomass plant
GB	Gas boiler
PV	Photovoltaic
OPEX	Operational expenditure

References

1. A European Green Deal. Available online: https://commission.europa.eu/strategy-and-policy/priorities-2019-2024/european-green-deal_en (accessed on 3 January 2023).
2. Federal Act on the Expansion of Energy from Renewable Sources (Renewable Energy Expansion Act). Available online: https://www.ris.bka.gv.at/Dokumente/Erw/ERV_2021_1_150/ERV_2021_1_150.html (accessed on 13 January 2023).
3. Netz Burgenland: Customer Service. Available online: <https://www.netzburgenland.at/kundenservice.html> (accessed on 11 January 2023).
4. Ruhnau, O.; Hirth, L.; Praktiknjo, A. Heating with wind: Economics of heat pumps and variable renewables. *Energy Econ.* **2020**, *92*, 104967. [[CrossRef](#)]
5. Dorotić, H.; Ban, M.; Pukšec, T.; Duić, N. Impact of wind penetration in electricity markets on optimal power-to-heat capacities in a local district heating system. *Renew. Sustain. Energy Rev.* **2020**, *132*, 110095. [[CrossRef](#)]
6. Golmohamadi, H.; Larsen, K.G.; Jensen, P.G.; Hasrat, I.R. Integration of flexibility potentials of district heating systems into electricity markets: A review. *Renew. Sustain. Energy Rev.* **2022**, *159*, 112200. [[CrossRef](#)]
7. Lamaison, N.; Collette, S.; Vallée, M.; Bavière, R. Storage influence in a combined biomass and power-to-heat district heating production plant. *Energy* **2019**, *186*, 115714. [[CrossRef](#)]
8. Wirtz, M.; Kivilip, L.; Remmen, P.; Müller, D. 5th Generation District Heating: A novel design approach based on mathematical optimization. *Appl. Energy* **2020**, *260*, 114158. [[CrossRef](#)]
9. Quaggiotto, D.; Vivian, J.; Zarrella, A. Management of a district heating network using model predictive control with and without thermal storage. *Optim. Eng.* **2021**, *22*, 1897–1919. [[CrossRef](#)]
10. Ummels, B.C.; Gibescu, M.; Pelgrum, E.; Kling, W.L.; Brand, A.J. Impacts of wind power on thermal generation unit commitment and dispatch. *IEEE Trans. Energy Convers.* **2007**, *22*, 44–51. [[CrossRef](#)]
11. Zheng, W.; Hou, Y.; Li, Z. A Dynamic Equivalent Model for District Heating Networks: Formulation, Existence and Application in Distributed Electricity-Heat Operation. *IEEE Trans. Smart Grid* **2021**, *12*, 2685–2695. [[CrossRef](#)]

12. Zheng, W.; Hill, D.J. Distributed Real-Time Dispatch of Integrated Electricity and Heat Systems with Guaranteed Feasibility. *IEEE Trans. Ind. Inform.* **2022**, *18*, 1175–1185. [[CrossRef](#)]
13. Koller, M.; Hofmann, R. Mixed-Integer Linear Programming Formulation of Combined Heat and Power Units for the Unit Commitment Problem. *J. Sustain. Dev. Energy Water Environ. Syst.* **2018**, *6*, 755–769. [[CrossRef](#)]
14. Wirtz, M.; Neumaier, L.; Remmen, P.; Müller, D. Temperature control in 5th generation district heating and cooling networks: An MILP-based operation optimization. *Appl. Energy* **2021**, *288*, 116608. [[CrossRef](#)]
15. von Rhein, J.; Henze, G.P.; Long, N.; Fu, Y. Development of a topology analysis tool for fifth-generation district heating and cooling networks. *Energy Convers. Manag.* **2019**, *196*, 705–716. [[CrossRef](#)]
16. Barone, G.; Buonomano, A.; Forzano, C.; Palombo, A. A novel dynamic simulation model for the thermo-economic analysis and optimisation of district heating systems. *Energy Convers. Manag.* **2020**, *220*, 113052. [[CrossRef](#)]
17. Li, X.; Li, W.; Zhang, R.; Jiang, T.; Chen, H.; Li, G. Collaborative scheduling and flexibility assessment of integrated electricity and district heating systems utilizing thermal inertia of district heating network and aggregated buildings. *Appl. Energy* **2020**, *258*, 114021. [[CrossRef](#)]
18. Klimarückblick Burgenland. 2021. Available online: https://ccca.ac.at/fileadmin/00_DokumenteHauptmenue/02_Klimawissen/Klimastatusbericht/KSB_2021/Klimarueckblick_Burgenland_2021.pdf (accessed on 25 January 2023).
19. EXAA Energy Exchange Austria with 4 Auctions. Available online: <https://www.exaa.at/> (accessed on 3 January 2023).
20. Austrian Gas Price Index. Available online: <https://www.energyagency.at/fakten/gaspreisindex> (accessed on 3 January 2023).
21. “Energy from Biomass” Index. Available online: <https://www.biomasseverband-ooe.at/fachinfo-links/index-energie-aus-biomasse.html> (accessed on 3 January 2023).
22. Hart, W.E.; Watson, J.P.; Woodruff, D.L. Pyomo: Modeling and solving mathematical programs in Python. *Math. Program. Comput.* **2011**, *3*, 219–260. [[CrossRef](#)]
23. Hilpert, S.; Kaldemeyer, C.; Krien, U.; Günther, S.; Wingenbach, C.; Plessmann, G. The Open Energy Modelling Framework (oemof)—A new approach to facilitate open science in energy system modelling. *Energy Strategy Rev.* **2018**, *22*, 16–25. [[CrossRef](#)]

Disclaimer/Publisher’s Note: The statements, opinions and data contained in all publications are solely those of the individual author(s) and contributor(s) and not of MDPI and/or the editor(s). MDPI and/or the editor(s) disclaim responsibility for any injury to people or property resulting from any ideas, methods, instructions or products referred to in the content.